PROCEEDINGS, 48th Workshop on Geothermal Reservoir Engineering
Stanford University, Stanford, California, February 6-8, 2023
SGP-TR-224

Geothermal mapping and remote sensing of thermal anomalies at Grændalur area, Hveragerði, SW Iceland

Muanza P.[1], Jónsdóttir I.[2], Kristinsson S.[3], Einarsson G.[3], and Björnsson G.[4]

[1] General Geology Department, Geological and Mining Research Center (CRGM), BP. 898 kin1, 44 Av. De La Démocratie, Kinshasa, DR Congo
[2] Faculty of Earth Sciences, University of Iceland, Sæmundargata 2, 102 Reykjavík, Iceland
[3] Iceland GeoSurvey (ISOR), Urðarhvarf 8, 203 Kópavogur, Iceland
[4] Warm Arctic, Iceland
muanzapatrick@gmail.com

Keywords: Geothermal mapping, TIR remote sensing, thermal anomalies, Grændalur geothermal field

ABSTRACT

This paper consists of geothermal mapping and identification of thermal anomalies using remote sensing in the Grændalur valley. This region is located in southwest Iceland, immediately north of the town of Hveragerði. It is located at the contact of the eastern margin of the Western Volcanic Zone (WVZ) and the South Icelandic Seismic Zone (SISZ). The area is seismically active, the most recent significant earthquake swarm occurred on May 29, 2008 with magnitudes of 6.3 and 5.5 between the towns of Selfoss and Hveragerði. The Grændalur valley is one of the areas in the Hveragerði region with intense geothermal activity. Geothermal mapping has been carried out in this area to map surface geothermal manifestations such as hot and warm springs, mud pools, fumarole, steam vents, steaming ground and structures. Remote optical sensors (Landsat and ASTER satellite images) were used to identify thermal anomalies in this area. The analysis of thermal anomalies made on daytime and nighttime satellite images from 2005 to 2020 has detected a new geothermal activity in the north near the center that would have certainly been created after the earthquakes of May 29, 2008. The thermal infrared (TIR) image taken with a TIR camera carried by a DJI Matrice 200 drone with a Zenmus XT thermal camera at 120 m height, was compared with temperature measurements taken directly on the ground after the flight to calibrate the TIR image for accuracy. The TIR image was used to identify and estimate the surface temperature of a geothermal manifestation whose accessibility was difficult. The surface temperature index of this geothermal manifestation is about 43°C.

1. INTRODUCTION

The Grændalur valley is one of the geothermal fields of the Hengill Central volcano and it is located about 6 km north of Hveragerði town. The Hveragerði town is located about 45 km southeast of Reykjavik, the capital of Iceland. The Grændalur valley is in the Southern Iceland Seismic Zone (SISZ) mainly in its western part which is in contact with the western flank of the active plate boundary between the North American and Eurasian crustal plates.

In the Grændalur valley, geothermal activity is directly linked to the extinct Grændalur central volcano. This volcano is part of the Hengill volcanic system and has moved away from the center of the rift by the extension of the plate boundaries. This is one of the parts of the Hengill volcanic zone (Ingólfsson et al., 2008; Arnórsson, 1995a).

This study focuses on mapping surface geothermal manifestations and identifying thermal anomalies using thermal sensors. For geothermal mapping, the description and temperature measurement of geothermal manifestations were done in the field. For thermal analysis, we used thermal infrared (TIR) images obtained from satellites and drones. The analysis of the satellite images covering the period from 2005 to 2020 allowed us to identify the evolution of thermal anomalies in the Grændalur valley before and after the earthquake of May 2008.

In a geothermal area, the technique of processing the spatial resolution of the sensors described below using color images from different acquisition dates and DEM image for structures makes it possible to analyze the surface activity. It is a technique that can cover large areas and be applied in places where access is difficult. And the results of repeating this technique provide important information on the possible change at the surface that may be caused by geothermal activity. In this study, the results of this technique have allowed us to improve our knowledge of the evolution of geothermal activity in the Grændalur valley.

Currently in the world, the acquisition of images using drones has become essential and has increased. In this study, we used the drone for the acquisition of TIR images in a part of our study area. These images were then calibrated to provide us with estimated values of the surface temperature of the study area. Currently, the technology of using the drone can contribute significantly to the monitoring as well as the study of geothermal areas especially in areas where the accessibility seems to be difficult or dangerous.

2. GEOLOGICAL BACKGROUND OF GRÆNDALUR

Iceland is an elevated plateau that lies in the middle of the North Atlantic between Norway and Greenland 63°23'N and 66°30'N, and ~12 – 25°W. It covers about 350,000km2, about 103,000 km2 above sea level with a crust thickness of 10-14km (Thórdarson and Larsen, 2007; Thórdarson and Höskuldsson, 2002). Iceland is located at the junction of the Greenland-Iceland-Faeroes Ridge which would be the

Icelandic Hotspot Trail and the submarine Mid-Atlantic Ridge which is considered to be the constructive plate boundary between the Eurasian and American Plates.

The Icelandic basalt plateau is geologically young, and all of its rocks have formed over the past 25 million years. It rises more than 3000 m above the surrounding ocean floor (Thórdarson and Höskuldsson 2002). It is mainly composed of Holocene lavas (<0.01 Ma), subglacial hyaloclastites (0.01-0.78), Plio-Pliocene lavas (0.78-3 + 3 Ma) (Hardarson et al., 2008), and Tertiary plateau lavas (3.3-16 Ma) (Moorbath et al., 1968; Watkins and Walker, 1977; McDougall et al., 1984; Hardarson et al., 1997).

In Iceland, the main geological structures are volcanic systems. These systems are characterized by a volcanotectonic structure comprising a swarm of fissures and central volcano that cross the country. In each volcanic system, fissure swarms are represented by faults and open fissures that are aligned following to the host volcanic zone. The central volcanoes are the focal point of eruptive activity (Thórdarson and Larsen, 2007). In the country, there are two transcurrent slip zones and several rift zones. In the south of the country, the Reykjanes segment of the Mid-Atlantic Ridge comes on the shore at the Reykjanes Peninsula as an oblique rift zone and branches into the Western Volcanic Zone (WVZ) and through the South Iceland seismic zone (SISZ) oriented EW (Saemundsson, 1978). The Western Volcanic Zone (WVZ) is connected to the Eastern Volcanic Zone (EVZ) which extends northward and continues like the North Volcanic Zone (NVZ) through the South Icelandic Seismic Zone (SISZ) which is an EW transformation movement (Árnadóttir et al., 2008). The South Icelandic Seismic zone (SISZ), which is the site of strike-slip earthquakes, constitutes the lower limit of a bloc meeting the criteria of a microplate called Hreppar (Einarsson, 2008). About 30 periods of destructive earthquakes have been recorded in SISZ since 1164 AD. The South Iceland Seismic Zone (SISZ) releases the stress accumulated during strike-slip earthquakes of about magnitude 7 (Einarsson, 1991). A large earthquake of magnitude 7 occurred in the area in 1912 and two earthquakes of magnitude 6.5 in 2000 on June 17 and 21, respectively (Pedersen et al., 2003). These various earthquakes in the area have increased geothermal activity (Björnsson G. and al., 2001). It is a phenomenon that occurs at intervals of decades to centuries.

The East-West-trending South Southern Iceland Seismic Zone (SISZ) shows evidence of Holocene fracturing and geologic formations such as alluvial plains, glacial surfaces and postglacial lava flows which are all fractured along this zone of 15 km wide and 70 km long (Einarsson and Eiríksson, 1982; Einarsson et al., 1981, 2002; Clifton and Einarsson, 2005). The majority of the fractures in this zone are oriented NNE to NE and form echelon fracture left-stepping to the left with a northern trend.

The volcanic systems above are characterized by volcanic activity with the fissure swarms are directly related to the geothermal activity of Iceland (Bodvarsson, 1961; Gudmundsson and Jacoby, 2007; Thórdarson and Larsen, 2007). The geothermal systems in Iceland have been classified according to the temperature of the reservoir (Arnórsson et al., 2008; Axelsson et al., 2005; Bodvarsson, 1961; Fridleifsson, 1979); there are:

- low temperature systems (<150°C) are associated with fractures and faults, some of which are located in active fissure zones which cross obliquely the country and in older formations.
- high temperature systems (> 200°C) are located in the central parts of volcanic systems and in the region of central volcanoes.

The Grændalur valley that is in the Southern Iceland Seismic Zone (SISZ), is mainly composed of basaltic rocks mainly tholeiite ranging from picrite to olivine and andesites as well as surface deposits. These basaltic rocks are subglacially hyaloclastites and interglacial lava flows. They are in particular vitreous tuffs, hyalocrystalline tuffs with porphyritic tuffs and rocks with aphyric, fine or coarse grain to variably porphyritic. Hyaloclastic and lava in Grændalur area are covered by superficial deposits (Saemundsson K. et al., 1994).

The lithostratigraphy of the Grændalur region from oldest to newest is presented as follows (fig.1):

- Formation of Varmár: is the oldest and most widely encountered rock group in the region. It is subdivided into three units:

  1. Breccias and pods of basalt lava form the core of the Varmár Formation. This formation is characterized by pods and blocks of basalt with a tuff matrix, measuring tens of meters in width. These lava pods are dense, very fine-grained basalt without olivine of tholeiitic composition. They are elongated in an N-S direction.

  2. Hyaloclastite tuff: it is a formation composed essentially of tuff or tuff-rich breccia which form thick units in inclined layers. It is a vesicular hyaloclastite with a relatively coarse texture without being brecciated.

  In the Grændalur valley, heavily weathered glass is replaced by green chlorite and / or mixed layers of brown smectite.

  It is in this formation that an important geothermal activity occurs due to the superficial nature of the rock faces and / or the deposit zones of the rivers (Saemundsson and Fridleifsson, 1992).

  3. The lava flows.

- Tholeiitic lava: it is a formation of interglacial lava with fine grains and aphyric texture. They appear in the form of basalts articulated in irregular columns inclined 2-3° to the south.
- Kvíar basalt group: it is an interglacial formation which is essentially composed of lavas and breccias with a feldsparphyritic texture and often feldspar phenocrysts.
- Fluvial deposits: these are deposits that partly cover the Holocene lava flows in the plain in front of the valleys and others are found above some of the largest rock slides.

- Rock slides: they were certainly caused by large earthquakes linked to the SISZ. They are from the Holocene and cover much of the region.

Geological structures such as faults and fractures in the Grændalur region are mainly oriented NE-SW. But on the surface, these different structures are oriented NE-SW, NW-SE and N-S.

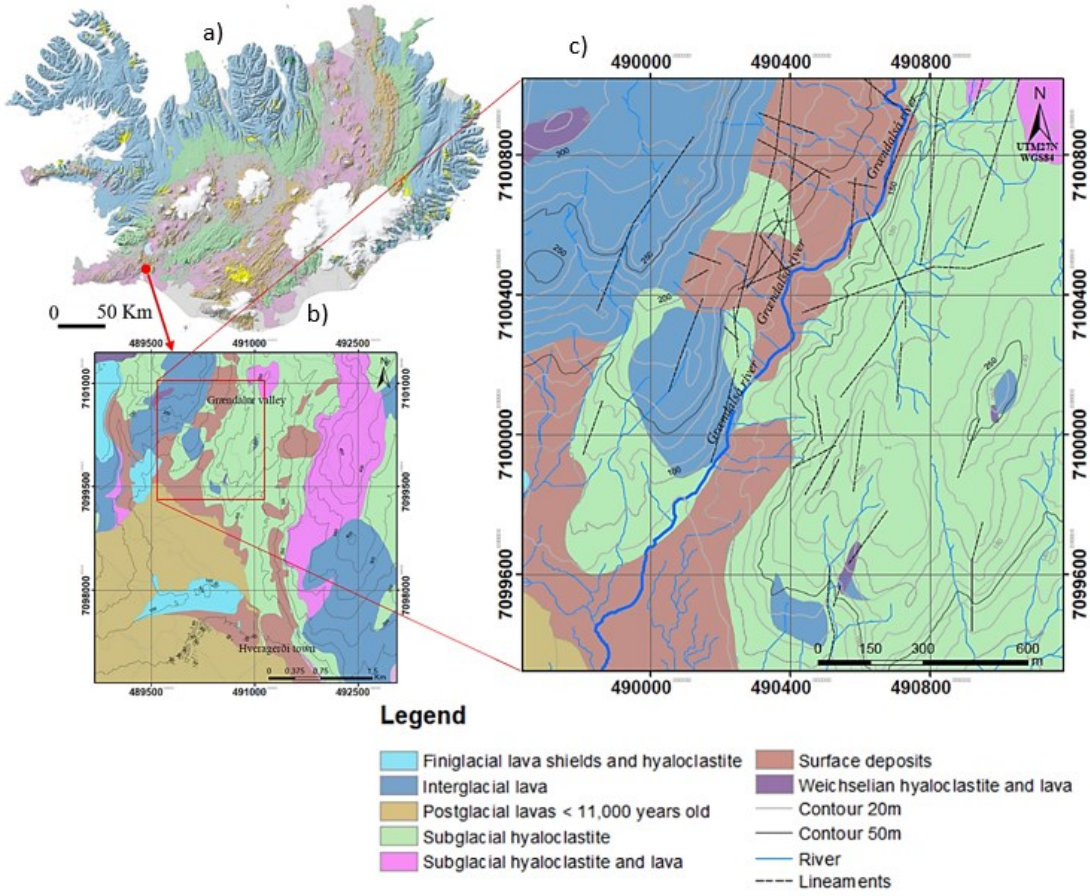

Figure 1: a: Map based on Geological map of Iceland. Iceland, 1:1.000.000 (Icelandic Institute of Natural History); b: Geological map of Hveragerði, c: Geological map of Grændalur valley (Saemundsson K. et al., 1994). Red circle and rectangle represent the approximate location of Grændalur valley.

3. METHODOLOGY

The geothermal mapping is a spatial representation of different types of geothermal manifestations that occur in the study area. To do this, the description of the geothermal manifestation was made in situ, the manifestations temperature measurements were performed using a digital thermometer and the positioning of their sampling points was done by GPS. After field work, the collected data were downloaded to a computer and edited by ArcGIS 10.6 software. The digital elevation model (DEM) 'IslandsDEMv0_2x2m_zmasl_isn2016_58' downloaded from the website www.lmi.is, was used to determine the geological structures of the area. The result is a geothermal map on a scale of 1: 8000 showing the geothermal manifestations and tectonic structures distribution in the valley.

The identification of thermal anomalies was made using Landsat and ASTER images. These images were downloaded from the USA Geological Survey (USGS) Earth Explorer web page. Their processing levels were L1 TP for Landsat and L1T for ASTER. Standard data for these levels is a radiometrically calibrated sensor, with systematic geometric corrections applied using spacecraft and DEM ephemeris data to correct for relief displacement and rotated to a Northup UTM projection. The scenes (daytime and nighttime) are provided in GeoTIFF format. The images used and their spectral and spatial resolution are shown in Tables 1. The collected data were downloaded to a computer and edited by ArcGIS 10.6, ENVI 5.3 and QGIS 3.16 software.

Table 1: List of satellite image data sets downloaded from the USGS Earth Explorer webpage.

Platform - Satellite	Acquisition date	Code
Landsat 7 ETM+	May 13th, 2007 (Daytime scene)	b
	July 16th, 2008 (Daytime scene)	c
Landsat 8 OLI & TIRS	April 23th, 2015 (Nighttime scene)	f
	August 31st, 2016 (Nighttime scene)	g
	October 21st, 2017 (Nighttime scene)	h
	October 24th, 2018 (Nighttime scene)	i
	May 04th, 2019 (Nighttime scene)	j
	November 14th, 2020 (Nighttime scene)	k
Terra - ASTER	December 15th, 2005 (Nighttime scene)	a
	February 25th, 2009 (Nighttime scene)	d
	May 20th, 2011 (Daytime scene)	e

The processing of the data for thermal anomaly mapping used in this study was done according to the procedure presented in figure 2.

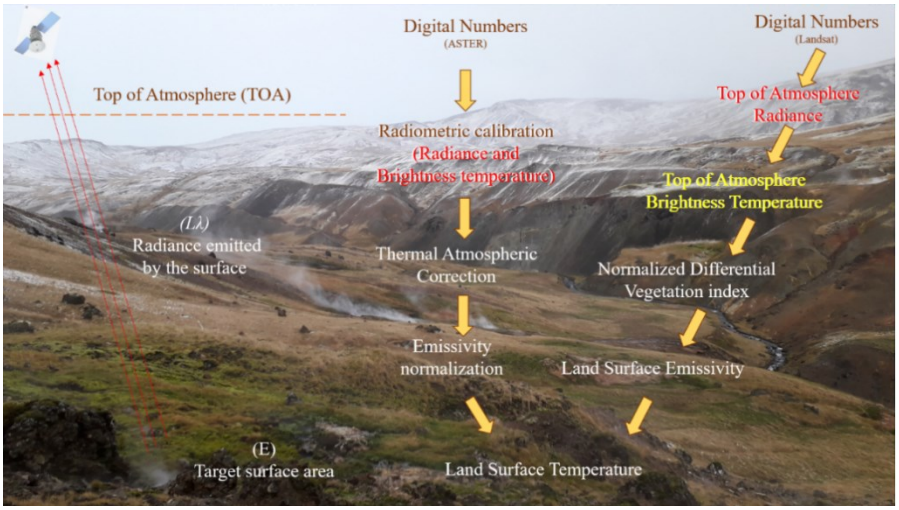

Figure 2: Data processing steps followed for thermal anomaly mapping retrieved by the satellite.

2.1 Estimation of LST values with Landsat

The estimation of LST values with Landsat is done using the thermal band 6 (Landsat 7) and band 10 (Landsat 8) according to the steps:

2.1.1 Top of atmosphere (TOA) radiance

Radiance includes the radiation reflected from the surface, in addition to the radiation that bounces in from neighboring pixels. The values in the selected band were converted to spectral radiance at the top of the atmosphere (TOA) ($L\lambda$) using the formula below (Gemitzi A., and al., 2021):

$$L\lambda = M_L * Qcal + A_L$$

where $L\lambda$, M_L, A_L *and Qcal* are spectral radiance (W/(m^2 * sr * µm)), radiance multiplicative scaling factor for the selected band taken from the metadata of the image, radiance additive scaling factor for the selected band from the metadata, the level 1 pixel value of selected band, respectively.

2.1.2 Top of atmosphere (TOA) Brightness Temperature

Brightness temperature is the temperature of a blackbody that would emit the same amount of radiation as the targeted body in a specified spectral band. The spectral radiance then converted to brightness temperature at the sensor (BT) with the following formula (U.S. Geological Survey, 2016 and Gemitzi A., and al., 2021):

$$BT = \frac{K_2}{ln\,(K_1/L\lambda + 1)} - 273.15$$

Where BT, $L\lambda$, K_1 and K_2 are TOA brightness temperature (◦C), TOA spectral radiance, Band 10 thermal conversion constant from the metadata (Landsat 8) or 666.09 for Landsat 7, Band 10 thermal conversion constant from the metadata (Landsat 8) or 1282.71 for Landsat 7, respectively.

Adding the absolute zero ~ -273.15 °C, is for converting from Kelvin degrees to Celsius degrees.

2.1.3 Land Surface Emissivity (LSE)

To better acquire LST estimates, it is important to know the ground emissivity or land surface emissivity (LSE (ε_λ)), which is the ability of a surface to transmit thermal energy to the atmosphere. It scales blackbody radiation according to Planck's law, to estimate the emitted radiation. It varies with vegetation conditions and surface roughness, which must also be known (Sobrino J.A. and al., 2004).

The Normalized Differential Vegetation Index (NDVI) is calculated following the formula:

$$\text{NDVI} = \frac{NIR - RED}{NIR + RED}$$

where NIR and RED are the Near Infrared and Red bands respectively represented by NIR (Band 5) and RED (Band 4) in Landsat 8, and NIR (Band 4) and RED (Band 3) in Landsat 7.

Estimation of LSE requires knowledge of vegetation proportion *Pv* which is calculated from the following equation (Gemitzi A., and al., 2021):

$$Pv = \left(\frac{NDVI - NDVI_{min}}{NDVI_{max} - NDVI_{min}} \right)^2$$

where NDVImax corresponds to fully vegetated surfaces if is > 0.6 and NDVImin refers to bare soil if is < 0.18 (Gemitzi A., Delampakis P. and Falalakis G., 2021; Sobrino et al., 2004; Sobrino and Raissouni, 2000). From the NDVI result of study area, NDVImin value is -0.00341793 and NDVImax value is 0.52948. Means that our study area is not totally covert by vegetation, it lies between a bare ground and a ground slightly covered with vegetation.

Next, LSE (ε_λ) is the average emissivity of an element of the surface of the earth calculated from NDVI values using the equation:

$$\varepsilon_\lambda = 0.004 * Pv + 0.986$$

where E and *Pv are* land surface emissivity (LSE), proportion of vegetation, respectively.

2.1.3 Land Surface Temperature (LST)

The LST is the radiative temperature which calculated using Top of atmosphere brightness temperature, wavelength of emitted radiance, LSE using equation (Anandababu D. and al., 2018):

$$\text{LST} = \left(\frac{\text{BT}}{1}\right) + \text{W} * \left(\frac{\text{BT}}{14380}\right) * ln\,(\varepsilon_\lambda)$$

where BT, W and ε_λ are TOA brightness temperature (°C), wavelength of emitted radiance, land surface emissivity (LSE), respectively.

2.2 Estimation of LST values with ASTER

The estimation of LST values with ASTER is done using the thermal band 14 according to the steps (Geospatial Solutions, Data & Imagery | Remote Sensing Technologies | L3Harris Geospatial):

2.2.1 Radiometric calibration

The radiometric calibration is a module used to calibrate image data (Pixel value) to radiance, reflectance, or brightness temperatures. For this case, radiance has been chosen.

To calculate it, the ASTER thermal bands are selected, and the module takes gains and offsets for each band by reading their values from the sensor metadata using the following equation:

$$L\lambda = Gain * Pixel\ value + offsets$$

where Lλ is Spectral radiance (W/(m2 * sr * μm))

2.2.2 Thermal Atmospheric Correction

After converting the thermal image data to radiance, atmospheric thermal correction is used to approximate and remove atmospheric contributions from the thermal infrared radiation data. It is done using the following equation (Harris A., 2013):

$$L(\lambda, T_s) = \frac{L(\lambda, T^*) - L_U(\lambda)}{\tau(\lambda)\,\varepsilon(\lambda)}$$

where $L(\lambda, Ts)$, $L(\lambda, T^*)$, $L_U(\lambda)$, $\tau(\lambda)$ and $\varepsilon(\lambda)$ are radiance of a blackbody at the surface, radiance arriving to the sensor (corresponding to brightness temperature), upwelling radiance from the atmosphere, transmissivity, emissivity, respectively.

The atmospheric correction is generated from an algorithm to determine the wavelength (used as reference wavelength) that most often has the maximum brightness temperature to calculate the atmospheric compensation. The radiance values of the reference blackbody are plotted against the measured radiances for each wavelength. The surface temperature of each pixel is estimated from the data and used to estimate the brightness temperature using the Planck function and assuming an emissivity of 1. Then a line is fitted to a cloud of radiation points with respect to the brightness temperature (Harris, 2017).

2.2.3 Emissivity normalization

After applying the atmospheric, thermal correction, emissivity normalization is used to calculate emissivity and temperature values from the thermal infrared radiation data. This technique calculates the temperature for every pixel and band in the data using a fixed emissivity value. With the Planck function, emissivity values are calculated using the highest temperature for each pixel.

For the thermal mapping in this study, we calculated the LST for thirteen satellite images. This LST corresponds to the temperature integrated over the pixel size of 30x30 m for Landsat and 90x90 m for ASTER.

The use of drones has become one of the most important image acquisition tools in the world. In this study, we used the DJI Matrice 200 drone carrying the TIR camera Zenmuse XT by FLIR. The TIR images acquired in TIFF format by the drone were used for the identification of thermal anomalies over the Grændalur Valley. Several TIR images were taken on April 30, 2021 (afternoons when the sun was not present) over the selected area at 120 m altitude and at a 20 m flight line interval.

Some ground temperature measurements of the area covered by the TIR images were taken with a digital thermometer for the calibration of the TIR images. These measurements were taken directly after the flight, at around depth of 5 cm in the ground and in the water. GPS coordinates were taken at each measurement point.

The Universal Transverse Mercator (UTM) projection system precisely from projection area 27 North and the World Geodetic System 1984 coordinate system were used for the geographic positioning of these data. Data processing was done using ArcGIS 10.6 software.

The steps followed for thermal anomaly mapping using a TIR camera carried by a drone are shown in the figure 3.

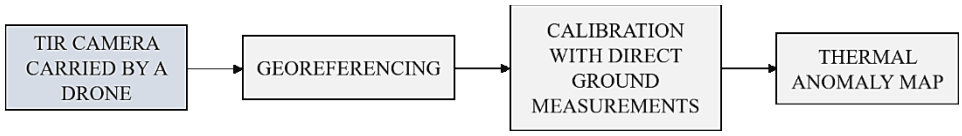

Figure 3: Steps followed for the thermal anomaly mapping using a TIR camera carried by a drone

4. RESULTS AND DISCUSSION

4.1 Geothermal mapping

The geothermal manifestations listed in the Grændalur area are hot ground, warm ground, steam vents, mud pools, fumaroles, cold springs, warm springs, and hot springs. Among all these geothermal manifestations, the most abundant are the hot springs.

4.1.1 Cold springs

In the Grændalur valley, all sources with a temperature below 15°C are classified in the category of cold sources. These sources can be groundwater that leans to the surface following fractures and faults. They are located at slightly higher altitudes than warm springs and hot springs.

4.1.2 Warm springs

The springs with temperatures between 15 and 50°C have been classified as warm springs in the study area. They are located at slightly higher altitudes than the hot springs. Around these sources, there are deposits of calcite. These sources, could be meteoric waters which circulate in the fractures and, are then heated by the steam circulating in the fractures and the faults and cooled maybe by clay alterations or by a diminishing geothermal activity.

4.1.3 Hot springs

In the Grændalur area, hot springs are the most abundant geothermal manifestations. These are sources that indicate a great geothermal activity in the region. They have a temperature above 50°C, some of which are boiling, and others are simply hot (fig.4). Some sources emit bubbles of CO_2 gas. The majority of these sources are colorless, others are whitish (coloring influenced by the presence of calcite) and others are brown (coloring influenced by the presence of clay particles). Around most of the hot springs, there are deposits of silica,

calcite and copper (in some springs); however, other hot springs are new and there are no deposits around. These hot springs could be connected to or influenced by the level of groundwater in the area.

4.1.4 Mud pools

Mud pools are geothermal manifestations that form in high temperature geothermal areas where water is scarce. In the Grændalur valley, the mud pools are near hot springs (fig.4). They are characterized by greyish boiling mud in a small basin formed by the little water available in these areas.

Figure 4: Hot spring and mud pool at Grændalur valley

4.1.5 Fumaroles/steam vents

These different geothermal manifestations are often found together and are sometimes linked to each other in the same place. Fumaroles and steam vents are well known, often with a hissing sound. They occasionally occur along tiny cracks or long fissures in clusters or non-systematic fields and thick deposits of pyroclastic flows. In active geothermal areas, there are fumarole / steam vents that emit steam and gases with different compositions, the most common contents are water vapor as dry steam, H2S and CO2 and other gases. The fumaroles which emit sulphurous gas are called Solfatara (Italian term coming from solfo which means sulfur).

4.1.6 Hydrothermal alteration, hot ground / steaming grounds and warm grounds

Generally, hydrothermal alteration is a process which occurs when there is interaction of a rock and a hydrothermal fluid, leading to the change of the physical and chemical components of the original rock by replacing its primary minerals with minerals secondary. Sampling the temperature of the altered soil in the area allowed us to subdivide this altered soil into two groups.

- Hot grounds/steaming grounds are characteristic soils of a zone of high geothermal activity, the temperature of which is above 50°C. They are easily identified by their whitish-brown, brownish-red color with deposits of gypsum, calcite, aragonite, and silica. In the study area, the highest temperature in the area was 98.6°C (fig.5).

Figure 5: Steaming ground in Grændalur valley.

- Warm grounds occur in a geothermal area and their temperature is below 50°C. They are easy to identify especially from the color of the vegetation (the moss) which generally changes from green to yellowish when the temperature increases. And in areas that do not have vegetative cover, warm soils have moist surfaces of smooth clay, and they are identified by a whitish coloration due to precipitation of calcite (Fig.6).

Figure 6: Yellowish green moss in warm ground in Grændalur valley

4.1.7 Relationship between the surface manifestations and the geological structures

In a geothermal area, the characterization of geological structures is very important because these structures are usually directly linked to geothermal manifestations. Generally, the information collected directly in the field and remote sensing allow us to observe and determine the direction of these structures. The analysis of the information collected in the Grændalur area from the remote sensing and the observation of the alignment of the geothermal manifestations (used as an indication for the presence of a geological structures), shows us that the faults and fractures found in this area have NE-SW, NS, EW, and NW-SE directions (fig.7).

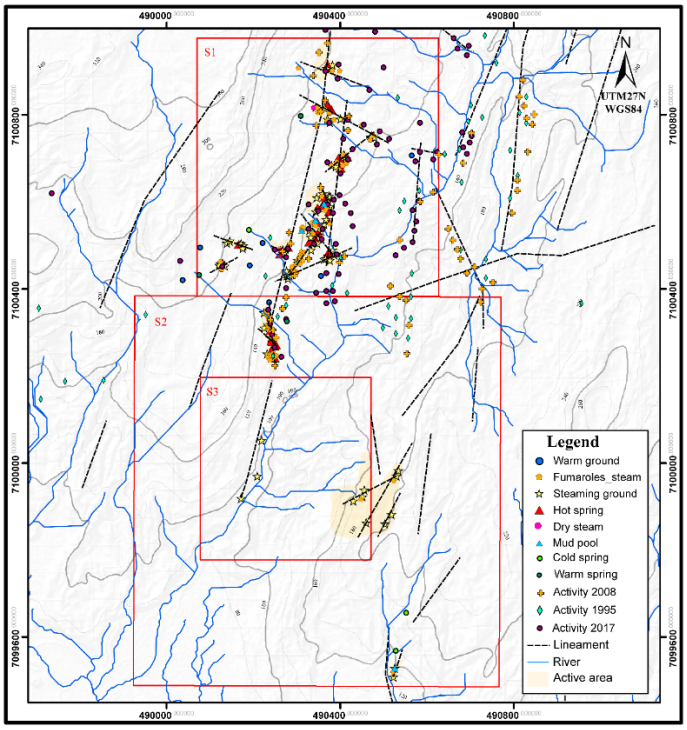

Figure 7: Geothermal mapping of Grændalur valley. Red rectangle showing the two sections location discussed below. This map has the same size as the Figure 1c.

As noted above, the geothermal manifestations found in the Grændalur valley are hot ground, warm ground, dry and steam vents, mud pools, cold springs, warm springs, and hot springs.

The figure 7 shows us the distribution of the different geothermal manifestations in the study area and we have subdivided them into 3 sections (S1, S2 and S3). The section 1 is divided into 2 regions (B1 and B2), the section 2 is divided into 3 regions (B3, B4 and B5) and the section 3 is the size of the area covered by Thermal image taken with the TIR camera.

- *Section 1 (regions B1 and B2)*

The distribution of geothermal manifestation in regions B1 and B2 is as follows (fig.8):

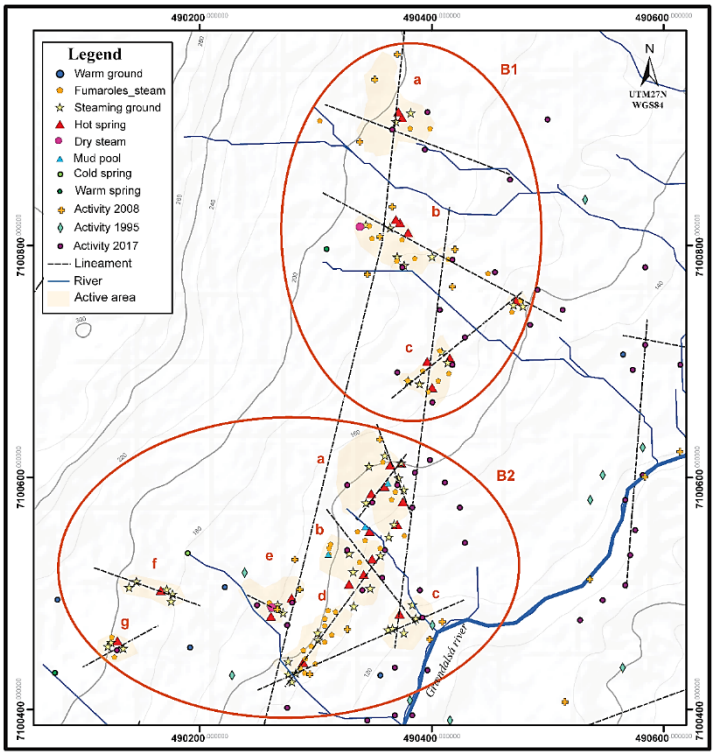

Figure 8: Geothermal manifestations and active geothermal areas in regions B1 and B2. The location of this area is S1 in Figure 7.

- In general, the geothermal manifestations are located on a slope in the region B1. In region B1a, on both sides we observe the boulder rock slides. The hot springs in this area have a temperature of around 78°C. There is also the fumaroles and the steaming ground which gives off an odor of sulfur (H_2S). The activity covers a semi-circular area with a radius of about 35m. Green and yellowish green foam is found all around the steaming ground. The geothermal manifestations follow a practically N-S direction in B1c and NW-SE direction in region B1b, there is a dry steam in this part which seems to be new.

- The region B2 is covered by an area of about 291x219m. Most geothermal manifestations in this region are grouped together in places, they are notably the steaming ground (surrounded by red-brownish, white and yellowish mineral precipitates) and the hot spring (with an average temperature of around 87°C) found in all the zones, there are fumaroles in zones B2a, B2b, B2d, B2e and B2g; the mud pools in regions B2a and B2b and the dry steam in the zone B2e. The geothermal manifestations follow a NW-SE and NE-SW direction. In zone B2a, yellowish green moss and dry grasses are easily observed, indicating new geothermal activity. The area B2f, appears to be new.

- *Section 2 (regions B3, B4 and B5)*

The distribution of geothermal manifestation in regions B3, B4 and B5 is as follows (fig.9):

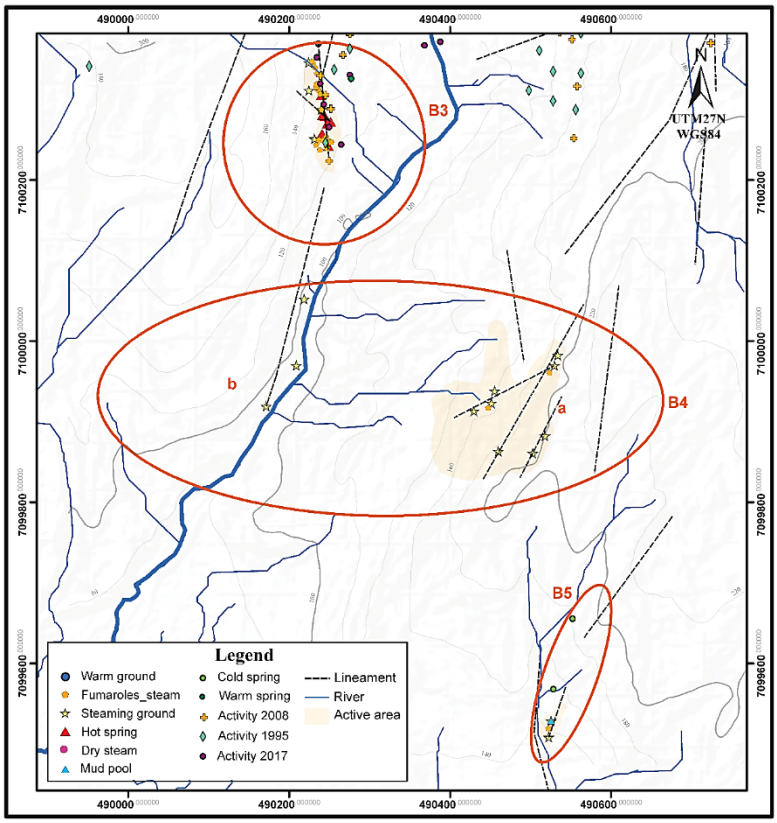

Figure 9: Geothermal manifestations, geological structures, and active geothermal areas in regions B3, B4 and B5. The location of this area is S2 in Figure 7.

- Region B3: it is an area of intense geothermal activity. These activities follow a practically NS direction and cover an area of about 150 x 25m. They are mainly composed of hot spring with a temperature around 98.2 °C, fumaroles, steaming grounds which are surrounded by deposits of white, yellowish and red-brownish minerals.

- Region B4: In this region, the geothermal events are the fumaroles and steaming grounds. In the B4a region, these manifestations are located on a steep slope and are cut off by a dike (fig.10). They are more remarkable for the color of the white mineral deposits that compose them. The B4b region is located on the small path which leads to the north of the site. The geothermal manifestations in this area are spaced along a N-S direction.

Figure 10: Geothermal manifestations in region B4.

- Region B5: In this region, geothermal manifestations are grouped together. The area covers an area of approximately 53 × 23 m. These geothermal manifestations follow a NE-SW direction. They are composed of steaming grounds with a temperature of 97.8°C and white, yellowish and red-brownish minerals, and fumaroles, one of which is directly connected to the mud basin above the slope. Next to the steaming grounds, there are green and yellowish-green moss.

Mapping of surface manifestations in the Grændalur valley, has revealed new manifestations that were created after major earthquakes of May 2008. Comparative analysis of the data presented in this thesis and previous work (before the earthquake by Saemundsson, 1995 and after earthquake by Thorbjörnsson et al., 2009; and Gemechu E.A., 2017) showed that there was an increase in geothermal activity in the area in 2008 immediately after the earthquake. Geothermal manifestations such as hot springs, boiling springs, fumaroles/steam vents, warm grounds, hot grounds and steaming grounds were identified towards the slightly elevated areas. In some parts of the study area, the geological features are covered by surface deposits, but the geothermal activity has been powerful to manifest itself at the surface revealing subsurface geological information such as alignments NE-SW, NS, EW, and NW-SE directions.

4.2 Identification of thermal anomalies

4.2.1 Satellite based LST retrieval

The thermal mapping done in this study required the calculation of LST for eleven satellite images (Daytime and nighttime scenes).

The figure 11 shows the temperature values in degrees Celsius. In these different maps, the highest temperatures corresponding to the surface geothermal areas and are represented in red and orange values. They show us the time series of thermal anomalies in the Grændalur valley using Landsat and ASTER imagery.

These thermal maps cover the period from 2005 to 2020. The observation of these different maps shows us a certain evolution of the spatial distribution of the thermal anomalies with time. In the area, the evolution is remarkable by the decrease of high thermal anomalies with time.

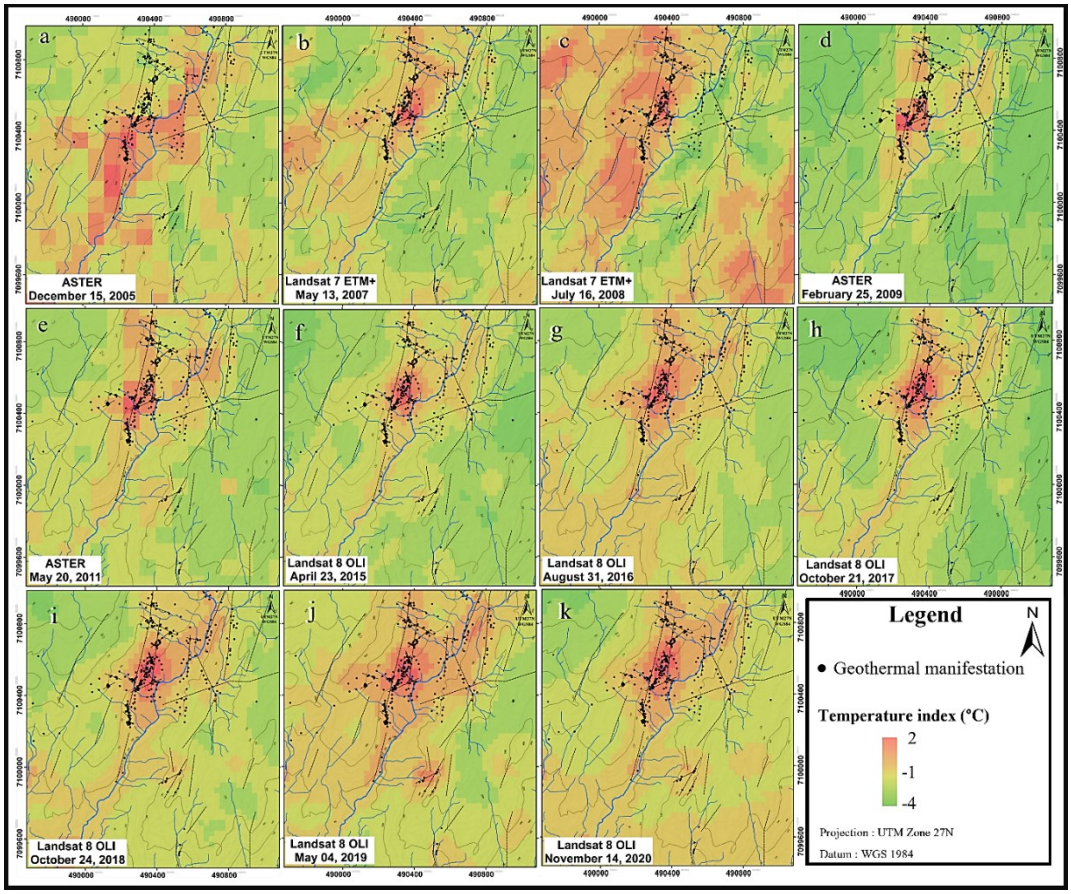

Figure 11: Evolution of thermal anomalies in the Grændalur geothermal field from 2005 to 2020. Thermal anomalies were categorized by standard deviations. The letters from a to k are related to the scenes (table 1 above).

Also, a thermal anomaly in the north close to the center is not detected on December 15, 2005 during the nighttime and May 13, 2007 during the daytime, but it was detected on July 16, 2008 during the daytime and from February 25, 2009 to November 14, 2020 during the nighttime (Fig.12).

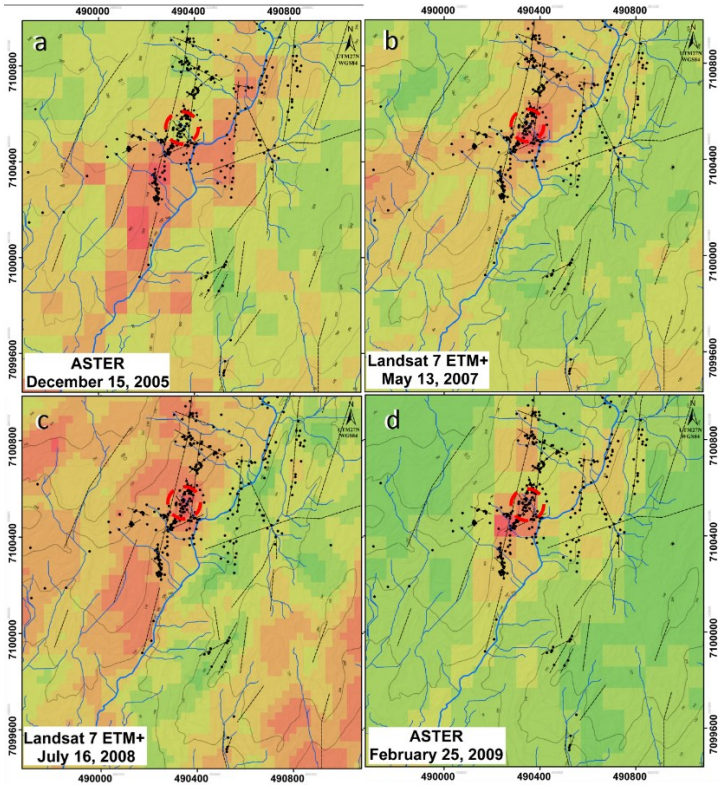

Figure 12: Thermal anomalies in the Grændalur geothermal field. The area where a thermal anomaly is not detected on December 15, 2005 and May 13, 2007 (within the red dotted line) (a and b) but detected from July 16, 2008 (c and d).

The thermal anomaly at Grændalur on December 15, 2005 and February 25, 2009 is not detected because the geothermal activity was not in that location at that time. This thermal anomaly seems to be a new geothermal activity that was created after the earthquake of May 29, 2008. As we said above, the date of May 29, 2008 was marked by an earthquake that had struck the region of Hveragerði. And this earthquake had increased the geothermal activity and revealed the presence of new geothermal manifestations in the area (Thorbjörnsson et al., 2009).

The estimation of the surface temperature made by the radiance analysis of the satellite images used in this study allowed us to identify the thermal anomalies on the valley of Grændalur. These different maps confirm the presence of geothermal manifestations and make the Grændalur valley one of the most active geothermal areas in Hveragerði.

To better apply remote sensing to geothermal exploration, it is important to have an objective and specially to take into account the size of the target to be analyzed or sought.

Generally, from its spatial resolution, the satellite-based remote sensor detects, and records thermal anomalies produced in the Grændalur geothermal field. The analysis of the images taken at different times allows us to have a good understanding of the evolution of thermal anomalies over time in a region. But one of the difficulties during the research is that of finding good images without cloud during the day or the night. In this study, we had this problem. We did not find good images taken at night especially for the Landsat 7 ETM+, this led us to make a good selection of images taken during the day for the Landsat 7 ETM+ and during the night for the Landsat 8 OLI and ASTER.

4.2.2 TIR camera carried by a drone

Currently, the technology of image acquisition using cameras carried by drones has become essential. However, the good precision and reliability of the results require the control in situ. For this study, thermal images taken at 120 m height were acquired in TIFF format from the TIR camera Zenmuse XT carried on the DJI Matrice 200 drone. For a good accuracy, some ground temperature measurements with the digital thermometer and their GPS points were taken directly after the flight to calibrate the TIR images (table 2).

Before the TIR images were taken, the 120 m height RGB images were taken using the RGB camera Zenmuse X4S carried by the DJI Matrice 200 drone and the orthomosaic image was created using Pix4d Mapper. In total, 193 RGB images captured in 3 flights and 198 thermal images captured in two flights.

In the orthomosaic image, the steaming grounds in the southern part of the Grændalur valley are visible (Fig. 13).

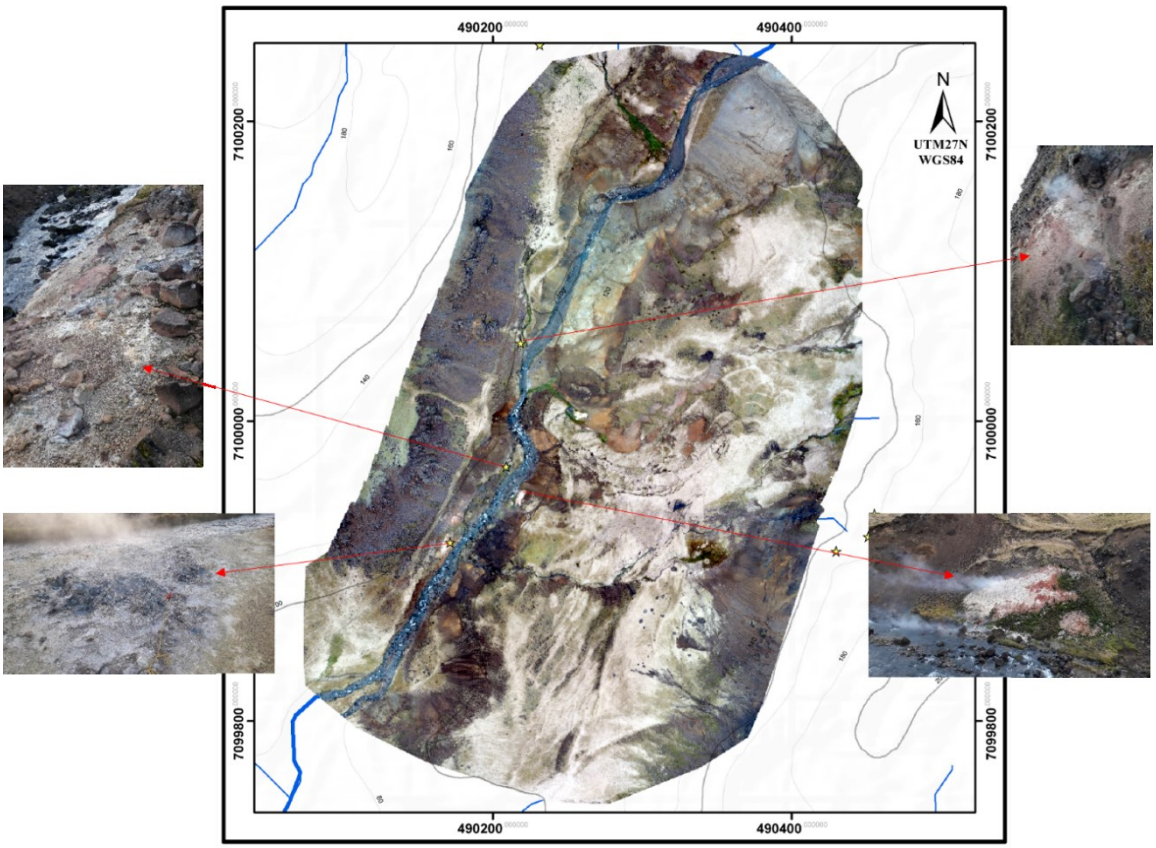

Figure 13: RGB mapping in the southern part of Grændalur valley showing the steaming grounds. The location of this area is S3 in Figure 7.

Immediately after the RGB images were taken, the thermal images from the TIR camera were taken with the TIR camera Zenmuse XT and then georeferenced using ArcGIS software. Figure 14 shows the thermal image, and the location of temperature measurement (1-5) on the ground.

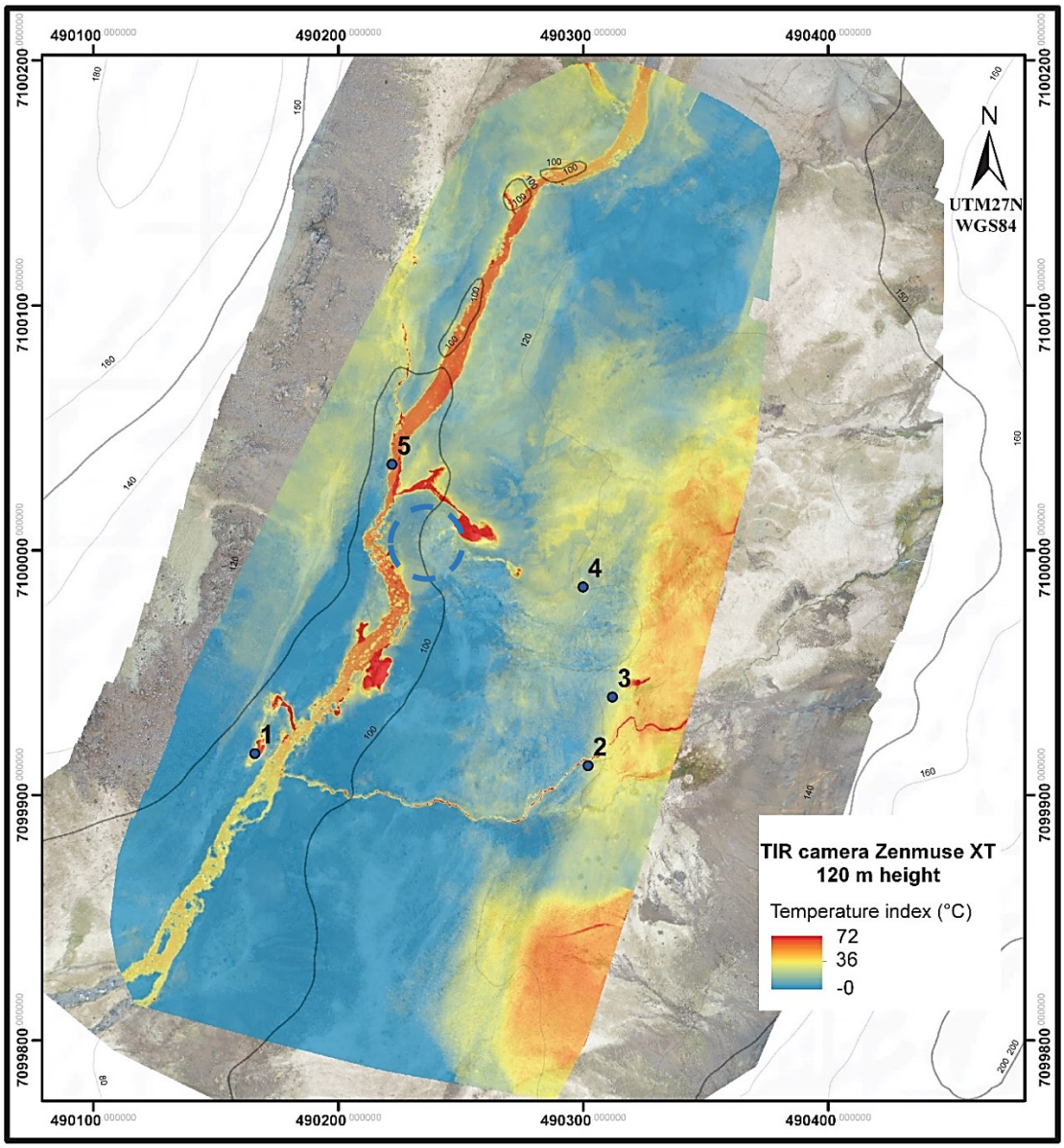

Figure 14: Thermal image taken with the TIR camera at 120 m. The blue labels are the locations where the direct temperature measurements were taken. The location of this area is S3 in Figure 7.

The temperature values of the thermal image pixels were then extracted using ENVI software at the same locations as the direct temperature measurements for the calibration (Table 2).

Table 2: Temperature measurements in the soil (water and steaming ground) and extracted from the TIR camera

Num.	Y_ UTM/27N	X_UTM/27N	Direct temperature measurement (T°C)	Temperature from the TIR camera (T°C)	Station
1	7099917	490166	65	33.49	Steaming ground
2	7099912	490302	34.9	30.98	Warm spring
3	7099940	490312	6.7	9.53	Ground
4	7099985	490300	6	9.46	Ground
5	7100035	490222	17.3	19.06	River

The difference in temperature between the direct temperature measurement and that extracted from the thermal image can be explained by the pixel size which generally increases with height. Since geothermal manifestations generally cover small areas, a thermal image taken from at a high elevation will have a large pixel size, but the pixel temperature will be integrated.

The temperature values that were extracted from the thermal image were plotted against the measurements that were taken directly on the ground at 5 cm depth. The graph obtained from the plots shows the linear relationship between the temperature values extracted from the thermal image and the direct temperature measurements (Fig. 15). The highest temperatures in this graph correspond to warm water and steaming ground.

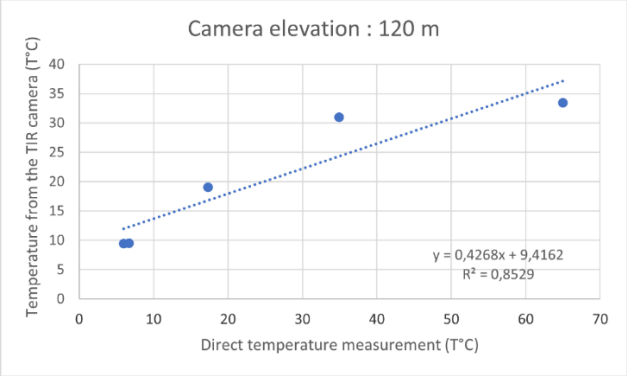

Figure 15: Plot of temperatures extracted from the thermal image at 120 m height and the direct temperature measurement at 5 cm.

The graph was made from Microsoft Excel and produced the linear regression equation with a coefficient of determination (R2) of 0.85. This regression equation was used to calibrate the thermal image (Fig.14).

Figure 16 shows the calibrated thermal image in degrees Celsius of the selected area with the highest temperature index in degrees Celsius of about 43°C. These high temperature locations correspond exactly to steaming grounds that we observed in the field and visualized in the RGB image (fig.13). Also, to estimate the temperature of a geothermal manifestation located in a place where the accessibility is difficult because it is located on a steep slope.

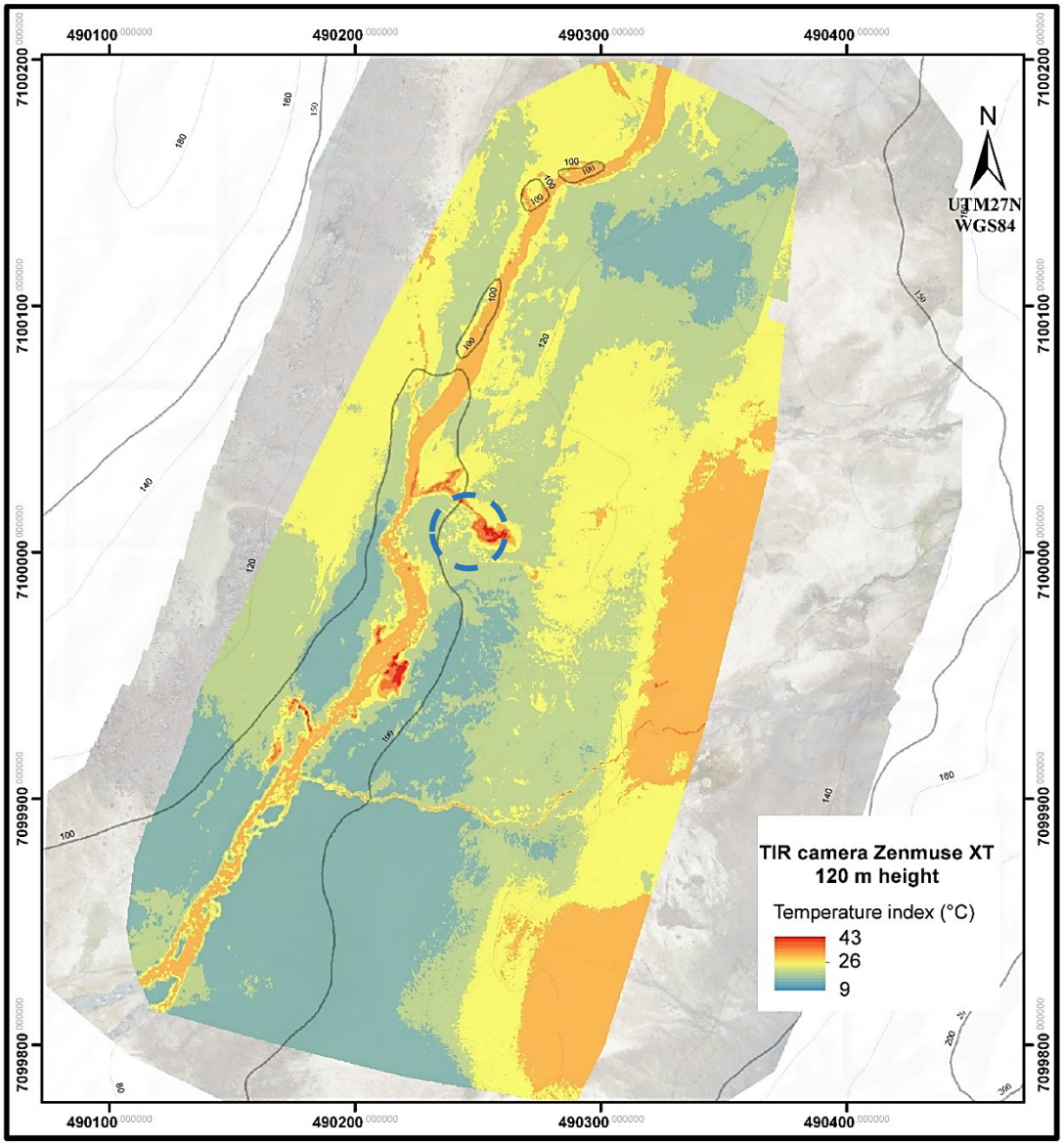

Figure 16: Thermal image calibrated taken with the TIR camera at 120 m. The blue dotted line is the geothermal manifestation located on a steep slope. The location of this area is S3 in Figure 7.

In this thermal map, the highest temperature index represented by the red value corresponds to the surface geothermal manifestations. The geothermal manifestation enclosed by blue dots shows the temperature pixel value of about 43°C at 120 m height.

The combined techniques of extracting land surface temperature from a satellite and a TIR camera carried by a drone produces effective results. It is used considering the size of the target to be detected. In the case of a geothermal area, geothermal manifestations such as steam vents, hot springs, mud pools, fumaroles, etc. that produce thermal anomalies are formed in small areas. In general, the size of these manifestations can vary from a few centimeters to a few meters. These anomalies are easily detected at a distance by satellite from the spatial resolution of the sensor. For Landsat, the resolution of the thermal infrared (TIR) is 30 x 30m per pixel, for ASTER, it is 90 x 90m and for the TIR camera, it depends on the height at which the image is taken (at 120m height, the spatial resolution is 14.7 x 15.1 cm). It is difficult, if not impossible, for a geothermal manifestation to reach 30 or 90m in length to cover the pixel size of Landsat and ASTER as a whole. This means that the temperature value obtained from the Landsat and ASTER pixel is actually an integrated temperature. Compared to Landsat and ASTER, the TIR camera has much higher spatial resolution and the size of the geothermal manifestation can cover its pixel size if the image is taken at a good height.

These techniques cannot determine the type of geothermal manifestations found in the study area. Generally, the satellite produces images on a regular basis. These images contain information about the time they were taken. The careful analysis of the images taken at different times allows to understand the evolution of the geothermal activity of the studied region. The analysis of satellite images from 2005 to 2020 of the Grændalur valley, shows us a certain the decrease of high thermal anomalies with time (Fig. 11). This decrease of the observed surface high thermal anomalies would be due to the decrease of the geothermal energy transfer to the surface. A thermal anomaly in the

center near the north was not detected until 2008 on the ASTER image nor on Landsat 7 ETM+. This anomaly has been detected since 2008 until 2020 on ASTER, Landsat 7 ETM+ and Landsat 8 OLI. It would have appeared after the earthquake of May 29, 2008.

To better monitor the possible change of geothermal activity (appearance or extinction of a geothermal manifestation) of an area, it is better to use remote sensors with a higher spatial resolution such as a thermal camera carried on a drone. The images produced by a thermal camera carried on the drone provide more detailed information because they can be taken at different altitudes. Regularly taking images from the thermal camera allows for careful monitoring of changes in geothermal activity and estimation of surface temperature after calibration with data taken in the field. In the Grændalur valley, the TIR image taken by a camera carried on the drone at 120m was calibrated with temperature measurements taken directly on the ground at 5cm depth. This calibrated TIR image was used to estimate the surface temperature index (43°C) of a geothermal manifestation located in a difficult to access area (fig.16).

This combined technique was used in the Sveifluháls-Krýsuvík high temperature Geothermal field to analyze time series of thermal anomalies from 2002 to 2017 and calculate the radiative heat flux (Ramírez-González L.M. et al., 2019).

CONCLUSIONS

Geothermal energy is one of the renewable energies generated in the ground and can be used directly for heating or transformed into electricity. The development of a geothermal project is done in several phases. One of the most important phases is geothermal exploration. In this phase, one of the most important methods is geological investigation. This method is done by two approaches: direct and indirect. The direct approach requires a field trip to make detailed maps, among which is geothermal mapping. The indirect approach is the spatial analysis by remote sensing.

The geothermal mapping of the Grændalur valley reveals the presence of geothermal manifestations such as hot springs, warm springs, fumaroles/steam vents, mud pools, hydrothermal alteration, hot ground, steaming ground and warm grounds. These geothermal manifestations follow NE-SW, N-S, E-W, and NW-SE oriented alignments that inform us about the direction of faults and fractures covered by the surface deposits.

The processing of TIR bands of Landsat and ASTER satellite images covering the period from 2005 to 2020 and the thermal image taken by a camera carried on the drone, allowed to analyze the spatial and temporal distribution of surface thermal anomalies in the Grændalur valley. The results obtained allowed us to:

identify the presence of a thermal anomaly that did not exist before the year 2008. This anomaly certainly appeared after the earthquakes of May 29, 2008 which had opened the door to a new geothermal manifestation and closed the door to others that existed in the area.

identified and estimated at about 43°C the temperature index of a thermal anomaly existing in an area located on a steep slope in the southern part of the Grændalur valley from TIR images with high spatial resolution taken by a TIR camera carried on the drone at 120m high.

This study attests to the importance of geothermal mapping, which is one of the most important early phases in geothermal exploration, which allows the study and mapping of geothermal manifestations and their correlation with geological structures for better understanding of the geothermal activity of a region. Also, it demonstrates the effectiveness of the analysis, processing and use of combined techniques of extraction of TIR images from satellite space sensors at different resolutions, taken at different times and that of the TIR image taken from the TIR camera carried on the drone in a geothermal area. This combination allows to cover large areas and detect thermal anomalies provided by geothermal manifestations.

The acquisition and regular analysis of these TIR images allow to monitor with great attention the possible changes of the surface geothermal activity in a geothermal area, especially for those located in a seismic area.

This combined technique can also be applied to the monitoring of an active volcano, by regularly analyzing TIR images of the volcanic area to detect possible changes in thermal anomalies provided by geothermal manifestations located in the area. These can provide information about a possible magma upwelling.

ACKNOWLEDGMENTS

We would like to thank the Centre de Recherches Géologiques et Minières (CRGM) through the General Director Professor Kanda Nkula for granting us the opportunity that made this study possible.

We sincerely thank the reviewers whose comments and suggestions significantly improved this manuscript.

The project was funded by the GRÓ–Geothermal Training Program as part of a MS fellowship.

REFERENCES

Árnadóttir T., Geirsson H., and Jiang W.: Crustal deformation in Iceland: Plate spreading and earthquake deformation. *Jökull,* **58**, (2008), 67 pp.

Arnórsson S.: Geothermal systems in Iceland; structures and conceptual models I, high temperature areas. *Geothermics,* **24**, (1995a), 561-602.

Anandababu D., Purushothaman B. M. and Suresh B.S.: Estimation of Land Surface Temperature using LANDSAT 8 Data. *International Journal of Advance Research, Ideas and Innovations in Technology*, (2018).

Axelsson G., Björnsson G., Egilson T., Flóvenz O. G., Gautason B., Hauksdóttir S., Ólafsson M., Smárason O. B. and Sæmundsson K.: Nature and properties of recently discovered hidden low-temperature geothermal reservoirs in Iceland. *Proceeding, World Geothermal Congress* 2005, Antalya, Turkey, (2005), 10 p.

Björnsson G., Flovenz Ó.G., Saemundsson K. and Einarsson E.H.: Pressure changes in Icelandic geothermal reservoirs associated with two large earthquakes in June 2000. *Proceedings,* Twenty-Sixth Workshop on Geothermal Reservoir Engineering, Stanford University, California, USA, 2001.

Bodvarsson G.: Physical characteristics of natural heat resources in Iceland. *State Electricity Authority*, Reykjavik, Iceland, G/6, (1961), 82-89.

Clifton A.E., and Einarsson P.: Styles of surface rupture accompanying the June 17 and 21, 2000 earthquakes in the South Iceland seismic zone. *Tectonophysics*, (2005), 396, 159 pp.

Einarsson P.: Earthquakes and present-day tectonism in Iceland. *Tectonophysics,* 189, (1991), 261-279.

Einarsson P.: Plate boundaries, rifts and transforms in Iceland. *Jökull,* 58, (2008), 35-58.

Einarsson P., and Eiríksson J.: Earthquake fractures in district and Rangárvellir in south Iceland seismic zone. *Jökull,* 32, (1982), 113-119.

Einarsson P., Böttger M., and Thorbjörnsson P.: *Faults and fractures of south Iceland Seismic zone near Thjórsá*. Landdsvirkjun, Reykjavík, report LV-2002/090, (2002), 8p.

Fridleifsson B. I.: Geothermal Activity of Iceland. *National Energy Authority*, Reykjavik. *Jökull,* 29, (1979), 47p.

Gemechu E.A.: Geothermal exploration in Grændalur valley, Hveragerði, S-Iceland. Report 11 in: *Geothermal training in Iceland 2017.* UNU-GTP, Iceland, (2017).

Gemitzi A., Delampakis P. and Falalakis G.: Detecting geothermal anomalies using Landsat 8 thermal infrared remotely sensed data. *International Journal of Applied Earth Observation and Geoinformation*, Volume 96, (2021), 102283**.**

Gudmundsson M.T., and Jacoby, W.: Hotspot Iceland: An introduction. *J. Geodynamics, 43-1*, (2007), 1-5pp.

Hardarson, B.S., Fitton, J.G., and Hjartarson, A.: Tertiary volcanism in Iceland. *Jökull,* 58, (2008), 161-178pp.

Hardarson B.S., Fitton J.G., Ellam R.M., and Pringle M.S.: Rift relocation-a geochemical and geochronological investigation of a paleo-rift in northwest Iceland. *Earth Planet. Sci. Lett.,* 153, (1997), 181-196.

Harris, A.: Thermal Remote Sensing of Active Volcanoes: A User's Manual. *Cambridge University* Press. ISBN 978-0-521-85945-5 Hardback, (2013), 756 p.

Harris A.: Geospatial Solutions, Documentation Center Using ENVI. Retrieved February-November 2017 from http://www.harrisgeospatial.com/docs/, (2017).

Ingólfsson Ó., Sigmarsson O., Sigmundsson F., and Símonarson L.: The dynamic geology of Iceland. *Jökull,* 58, (2008), 1–2.

McDougall I., Kristjánsson L., and Saemundsson K.: Magnetostratigraphy and geochronology of northwest Iceland. *J. Geophys. Res.,* 89(B8), (1984), 7029-7060.

Moorbath S., Sigurdsson H., and Goodwin R.: K-Ar ages of oldest exposed rocks in Iceland: *Earth and Planetary.* Science Letters, 4, (1968) 197-205.

Pedersen, R., S. Jónsson, Þ. Árnadóttir, F. Sigmundsson and Feigl K.: Fault slip distribution of two Ms=6.6 earthquakes in South Iceland from joint inversion of InSAR and GPS. *Earth Planet.* Sci. Lett, (2003), in press.

Ramírez-González L.M., Aufaristama M., Jónsdóttir I., Höskuldsson Á., Þórðarson Þ., Proietti N.M., Kraft G. and McQuilkin J.: Remote sensing of surface Hydrothermal Alteration, identification of Minerals and Thermal anomalies at Sveifluháls-Krýsuvík high-temperature Geothermal field, SW Iceland. *IOP Conf. Series: Earth and Environmental Science 254 (2019) 012005.* doi:10.1088/1755-1315/254/1/012005.

Saemundsson K.: Fissure swarms and central volcanoes of the neovolcanic zones of Iceland. *Geol. J., Sp. Issue,* 10, (1978), 415-432.

Saemundsson K., and Fridleifsson G.Ó.: *The Hveragerði central volcano, geological description.* Orkustofnun, Reykjavík, report OS-92063/JHD-35 B (in Icelandic), (1992), 25 pp.

Saemundsson K., Þórólfur H. Hafstað og Freystein Sigurðsson: Hveragerði og nágrenni. Jarðfræði-, jarðhita- og grunnvatnskort 1:5.000. Orkustofnun. Unnið fyrir Hveragerðisbæ, (1994).

Saemundsson, K.: Geological map of the Hengill area 1:50,000. *Orkustofnun*, Reykjavík, Iceland, (1995).

Sobrino, J.A., Raissouni, N., 2000: Toward remote sensing methods for land cover dynamic monitoring: application to Morocco. *Int. J. Remote Sens.* 21, 353–366.

Sobrino, J.A., Jiménez-Muñoz, J.C., Paolini, L., 2004: Land surface temperature retrieval from LANDSAT TM 5. *Remote Sens. Environ.* 90, 434–440.

Thorbjörnsson D., Saemundsson K., Kristinsson S.G., Kristjánsson B.R, and Ágústsson K, 2009: *Southern lowland earthquakes May 29th, 2008, effect of groundwater level, geothermal activity and fractures*. ÍSOR – Iceland GeoSurvey, Reykjavík, report ÍSOR-2009/028 (in Icelandic), 42 pp.

Thórdarson T. and Larsen G., 2007: Volcanism in Iceland in historical time: Volcano types, eruption styles and eruptive history. Journal of Geodynamics 43, 118-152.

Thórdarson T., and Höskuldsson A., 2002: Classic Geology in Europe 3: Iceland, Terra *Publishing, Hertfordshire,* England.

Watkins N.D., and Walker G.P.L., 1977: Magnetostratigraphy of Eastern Iceland. *Am. J. Sci., 277,* 513-584.